A&A 473, 551–559 (2007)
DOI: 10.1051/0004-6361:20077398

Astronomy & Astrophysics

Long-term pulse profile study of the Be/X-ray pulsar SAX J2103.5+4545

A. Camero Arranz[1], C. A. Wilson[2], M. H. Finger[2,3], and V. Reglero[1]

[1] GACE, Instituto de Ciencias de los Materiales, Universidad de Valencia, PO Box 20085, 46071 Valencia, Spain
e-mail: Ascension.Camero@uv.es
[2] VP62, National Space Science and Technology Center, 320 Sparkman Drive, Huntsville, AL 35805, USA
[3] Universities Space Research Association, Huntsville, AL 35805, USA

Received 3 March 2007 / Accepted 17 July 2007

ABSTRACT

Aims. We present the first long-term pulse profile study of the X-ray pulsar SAX J2103.5+4545. Our main goal is to study the pulse shape correlation either with luminosity, time or energy.
Methods. This Be/X-ray binary system was observed from 1999 to 2004 by *RXTE* PCA, and by *INTEGRAL* from 2002 to 2005, during the Performance and Verification (PV) phase and the Galactic Plane Scan survey (GPS). X-ray pulse profiles were obtained in different energy ranges. The long-term spectral variability of this source is studied. The long-term flux, frequency and spin-up rate histories are computed. A new set of orbital parameters are also determined.
Results. The pulse shape is complex and highly variable. Despite this fact, the strength of almost all the peaks increases with luminosity. In addition, an energy dependence pattern was found. Single, double, triple or even quadruple peaks pulse profile structure was obtained. It was confirmed that SAX J2103.5+4545 becomes harder when the flux is higher. The new orbital solution obtained is: $P_{\rm orb}$ = 12.66528 ± 0.00051 days, e = 0.401 ± 0.018, ω = 241.36 ± 2.18 deg and $a_x \sin i$ = 80.81 ± 0.67 lt-s.

Key words. X-rays: binaries – stars: pulsars: general – stars: individual: SAX J2103.5+4545 – stars: binaries: close – stars: emissions-line, Be

1. Introduction

SAX J2103.5+4545 is a Be High Mass X-ray Binary pulsar with an orbital period of 12.68 d (the shortest known in Be/X-ray binary systems) and X-ray pulsations of 358 s. These systems consist of a neutron star orbiting a Be companion, hence forming a Be/X-ray binary. Be stars are rapidly rotating objects with a quasi-Keplerian disk around their equator. The optical and infrared emission is dominated by the donor star and its equatorial disk, and it is characterized by spectral lines in emission (particularly those of the Balmer series) and IR excess. The standard model of a Be/X-ray binary ascribes the high-energy radiation to an accreting mechanism that takes place when the compact object interacts with the Be star's circumstellar disk, giving rise to an X-ray outburst.

This source was discovered by the *BeppoSAX* satellite (Hulleman et al. 1998). The X-ray spectrum (2–25 keV) was fitted by a power-law with a photon index of 1.27 ± 0.14 plus a photoelectric absorption at lower energies ($N_{\rm H}$ = 3.1 × 10^{22} cm^{-2}). The likely optical counterpart is a B0Ve star (V = 14.2) at a distance of 6.5 kpc (Reig et al. 2004). Using *XMM-Newton* data a quasi-periodic oscillation at 22.7 s was discovered by İnam et al. (2004). Baykal et al. (2002) found a correlation between spin-up rate and X-ray flux during the 1999 outburst. This suggests the formation of an accretion disk during periastron passage of the neutron star. However, SAX J2103.5+4545 is not a regular Be/X-ray system. For instance, it does not follow the Corbet $P_{\rm orb}/P_{\rm spin}$ correlation found in other accreting pulsar systems. Previous works of SAX J2103.5+4545 during quiescence by Reig et al. (2005) showed that this is a very interesting case. They found that the source was emitting X-rays even after the complete loss of the circumstellar disk. On the other hand, Baykal et al. (2002) and İnam et al. (2004) found single and double peak pulse profiles respectively in the soft X-ray range. In the hard X-ray range, Filippova et al. (2004) found only a single peak profile. However, a double peak profile was then found by Falanga et al. (2005) and Sidoli et al. (2005). We find the overall picture of SAX J2103.5+4545 still puzzling.

As a review, this source has been analyzed previously by Hulleman et al. (*BeppoSAX*, 1998), Baykal et al. (2000, 2007) and İnam et al. (2004) (*RXTE*, *XMM-Newton*) (optical & IR wavelengths, 2004, 2005), Filippova et al. (optical wavelength; *RXTE*, *XMM-Newton*, *INTEGRAL*, 2004), Blay et al. (2004), Falanga et al. (2005) and Sidoli et al. (2005) only with *INTEGRAL* data, Blay (optical/X-ray correlation; *INTEGRAL* 2006) and Camero-Arranz et al. (2006) with *RXTE* & *INTEGRAL* .

We present a long-term pulse profile study, as well as a spectral and pulse-timing analysis of SAX J2103.5+4545 using data from both *INTEGRAL* and *RXTE* missions.

2. Observation and data reduction

The INTErnational Gamma-Ray Astrophysics Laboratory (*INTEGRAL*, Winkler et al. 2003) consists of three coded mask telescopes, the spectrometer SPI (20 keV–8 MeV), the imager IBIS (15 keV–10 MeV), and the X-ray monitor JEM-X

(4–3 keV), as well as the optical monitoring camera OMC (V, 500–600 nm).

SAX J2103.5+4545 has been detected by IBIS/ISGRI during the *INTEGRAL* PV phase and the GPS survey from 2002 to 2005 (MJD 52 618–MJD 53 356), with a total observing time of ∼860 ks. *INTEGRAL* data reduction was carried out with the Offline Scientific Analysis software, release 5.0, distributed by the ISDC (Courvoisier et al. 2003). A software description can be found in Goldwurm et al. (2003), Diehl et al. (2003), Wetergaard et al. (2003).

RXTE Bradt et al. (1993) carries 3 instruments on board. The Proportional Counter Array (PCA; Jahoda et al. 1996) is sensitive from 2–60 keV. The High Energy X-ray Timing Experiment (HEXTE; Gruber et al. 1996) extends the X-ray sensitivity up to 200 keV. Monitoring the long-term behavior of some of the brightest X-ray sources, the All Sky Monitor (ASM; Levine et al. 1996) scans most of the sky every 1.5 h at 2–10 keV.

SAX J2103.5+4545 was also observed with *RXTE* PCA and HEXTE from 1999 to 2004 (MJD 51 512.8–MJD 53 047.9), with a total observing time of ∼1900 ks. However, it is important to note that during that period there were two gaps with no observations taken by those instruments (MJD 51 900–MJD 52 000 and MJD 52 025–MJD 52 430). For each available observation, we have analyzed PCA Standard1 data (0.125 s time resolution, no energy resolution) for the light curves and Standard2 data (16 s time resolution, 129 channel energy resolution) for spectral analysis using FTOOLs 6.2. In addition, GoodXenon PCA data were selected for the pulse profile study, and HEXTE binned mode data from clusters A and B for the spectral analysis.

3. Data analysis and results

3.1. Pulse profile analysis

In order to study the long-term pulse profile dependence on luminosity, time or orbital phase we extracted 548 *RXTE* PCA Standard1 light curves in the 2–60 keV energy range. The background was not subtracted in this first step. Then, we corrected the times to the barycenter of the solar system, as well as for the orbital motion using the binary orbital parameters by Baykal et al. (2002). We constructed pulse profiles by fitting the data with a harmonic expansion in pulse phase (6 harmonics were used). Typically we use data spanning a 4000 s interval (∼11 pulse periods). Initially we used a simple phase model ($\phi(t_k) = \phi_0 + f_0(t_k - t_0)$; where f_0 is the pulse frequency at time t_0 and ϕ_0 is the phase at time t_0). The errors on the Fourier coefficients were corrected for the non-Poisson noise found in the power spectra (Wilson et al. 2002). In a later stage, a more precise quadratic-spline phase model was created, which was used to remake the profiles.

We have obtained 2–60 keV *RXTE* PCA pulse shapes varying from only single sinusoidal-like peak (phases 0.9–1), to profiles with two peaks (phases 0.7–0.9), and even occasionally with three (phases 0.5–0.7) and four peaks (0.2–0.5) (see Figs. 1, 2, or 3).

Taking consecutive pulse profiles in time during outbursts, and after visual inspection, we found a non correlated shape pattern from one outburst to another, and even different patterns either going up or down for a given outburst (see Fig. 1, where Relative Flux is the number of counts per second and per PCU relative to the mean rate). As we stated before, generally the shapes vary from a strong single sinusoidal-like peak to double. However, three or even four weaker peaks are often found in addition to the main one. This source showed the same arbitrary

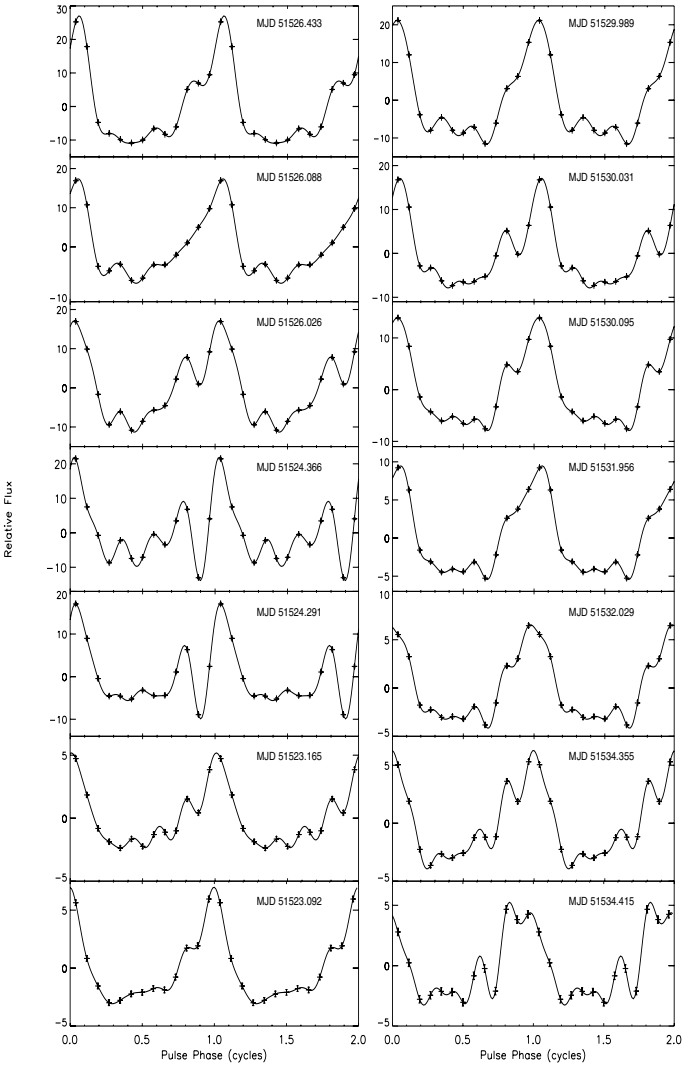

Fig. 1. *RXTE* PCA (2–60 keV) pulse profiles consecutive in time during outburst. Two cycles are plotted for clarity. The evolution of intensity of the first part of the outburst is plotted on the left column increasing *from bottom to top*. The fall is plotted on the right, with intensity decreasing *from top to bottom*.

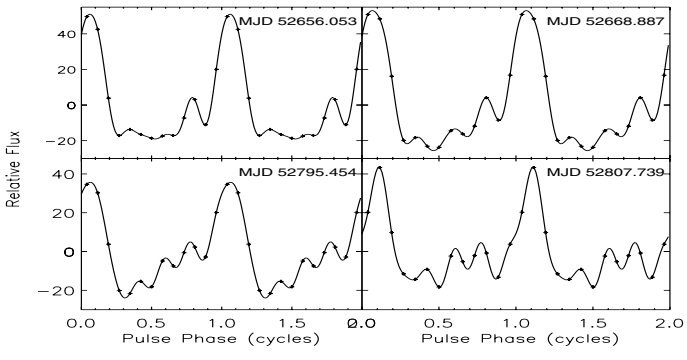

Fig. 2. PCA (2–60 keV) pulse profiles at the same orbital phase (0.73 ± 0.02 cycles) and at the same luminosity state ($5.62\pm0.04\times10^{+36}$ erg s^{-1}).

conduct when profiles are sorted by orbital phase (see Fig. 2). Moreover, we expected to obtain a base profile for a given X-ray luminosity. Nevertheless, we discovered a diversified range of shapes with no clear resemblance (see Fig. 3).

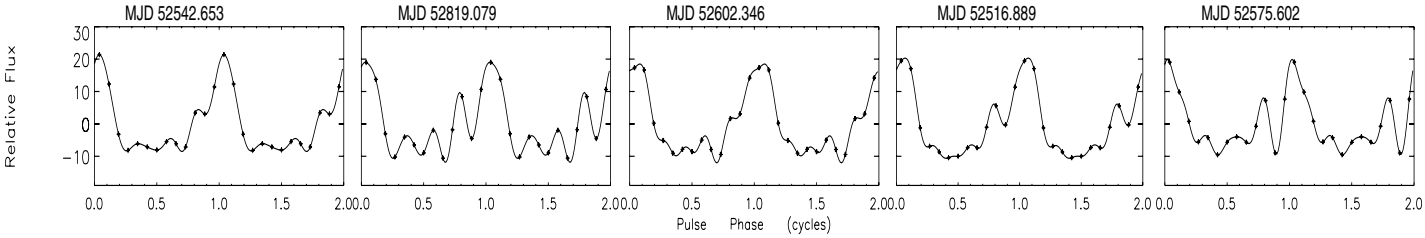

Fig. 3. *RXTE* PCA 2–60 keV pulse profiles at the same luminosity state ($L \simeq 2 \pm 0.6 \times 10^{+36}$ erg s^{-1}; see Fig. 4 *bottom*).

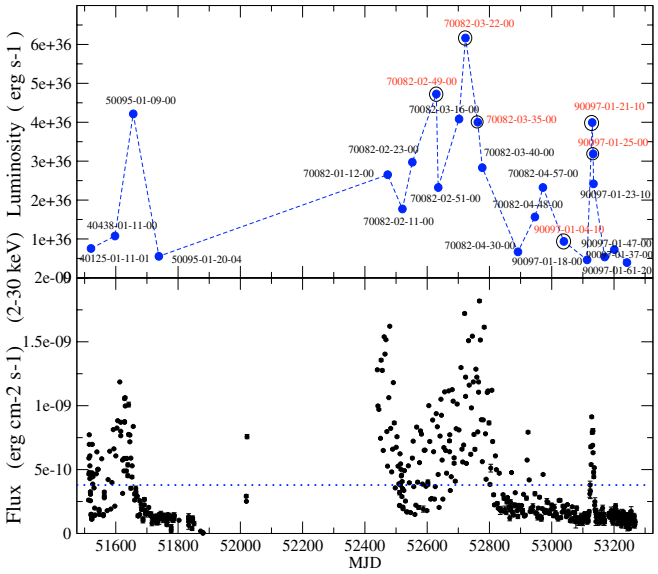

Fig. 4. *Top.* Sample of PCA observations selected for the pulse profile intensity analysis. An extra circle indicates the existence in addition of an *INTEGRAL* IBIS/ISGRI observation. *Bottom*. *RXTE* PCA flux in the 2–30 keV energy range. The horizontal dotted line denotes the luminosity level of $\simeq 4 \times 10^{+36}$ erg s^{-1}.

Table 1. Pulse period detections of SAX J2103.5+4545 with IBIS/ISGRI. The second column shows 0000the number of ScWs used for the computation in each epoch.

Epoch (MJD)	Number of ScWs	Pulse period (s)
52 619.299	6	–
52 630.755	49	354.927 ± 0.014
52 637.303	18	–
52 722.884	3	354.072 ± 0.014
52 761.947	35	353.478 ± 0.017
52 797.040	2	–
52 805.978	3	–
52 820.945	2	–
53 021.331	74	–
53 038.548	119	352.446 ± 0.019
53 041.996	21	–
53 102.514	3	–
53 130.288	77	352.350 ± 0.006
53 133.176	51	352.29 ± 0.01
53 188.993	2	–
53 258.517	3	–
53 333.056	6	–
53 349.280	5	–
53 354.965	4	–

In addition we have quantified the strength of all the peaks. We have defined the strength of one peak of the pulse profile as the ratio $(I_{\max} - I_{\rm np})/I_{\rm np}$, where $I_{\rm np}$ was defined as the "non-pulsed "flux at the middle point between the two adjacent minima of the peak. We have plotted this magnitude in time as well as versus the orbital phase and luminosity (2–60 keV rms flux) for 548 *RXTE* observations (see Fig. 5). The root-mean-square flux of each observation was estimated as $[\sum_{i=0}^{1}(a_{ih}^2 - a_{ih\rm err}^2))/2]^{1/2}$, where a_{ih} are the cosine and sine coefficients of the Fourier series for profile i and harmonic h, and $a_{ih\rm err}$ are the errors of those coefficients.

From Fig. 5 it appears that the strength of the four peaks increases with the luminosity.However, the correlation coefficients of the main, second, third and fourth peaks were 0.95, 0.83, 0.30 and 0.56, respectively (with significance values of their deviations from zero being 0, 1×10^{-41}, 0.0002, 2×10^{-14}). This suggests that all but the third are correlated with luminosity. In addition, computing the ratio of the main to the second peak of the pulse profile (P1/P2), and to the third (P1/P3) and to the fourth one (P1/P4), we found a wide range of the ratio values for a given luminosity state (see Fig. 6). This confirms our initial visual inspection, i.e., the pulse shapes vary with no clear pattern. On the other hand, we believed it was worthwile to compute also the correlation coefficients of P1/P2, P1/P3, P1/P4. They were all found to be ∼0.44, after rejecting some values with very large uncertainties. When we focused on the lower part of the flux range (rms flux from 0 to ∼10), there was only a slight improvement on the P1/4 correlation coefficient, with a value of ∼0.50.

Once we confirmed that no evident temporal, orbital or luminosity pulse shape correlations were found in the original PCA data sample in the 2–60 keV range, we decided to select only 24 goodXenon *RXTE* PCA observations for the energy dependence study. The chosen data set follows the long-term light curve behavior and covers MJD 51512.8 to 53 047.9 (see Fig. 4). The PCA background subtracted light curves were obtained in four energy ranges: 2.06–5.31 keV, 5.31–7.76 keV, 7.76–13.93 keV, 13.93–20.62 keV. Then, the same procedure was followed to construct the phases and then the profiles, as we described before. Typically, the duration of a *RXTE* PCA observation is about 3000 s and the profiles contain about 8 pulse cycles. To complete this study, we obtained a list of good events times per science window (ScW) with IBIS/ISGRI in the 20–60 keV energy band. Table 1 shows a summary of the detections and non detections with this instrument, as well as the number of ScWs used for making profiles. In Fig. 4 we marked in red (and an extra circle) those 6 points in which we also have an IBIS/ISGRI positive detection.

Figures 7 and 8 show the evolution of some of the PCA profiles in four energy bands (with energy increasing from top to bottom). As we already mentioned, the profiles present a prominent sinusoidal-like peak among other features. These can vary

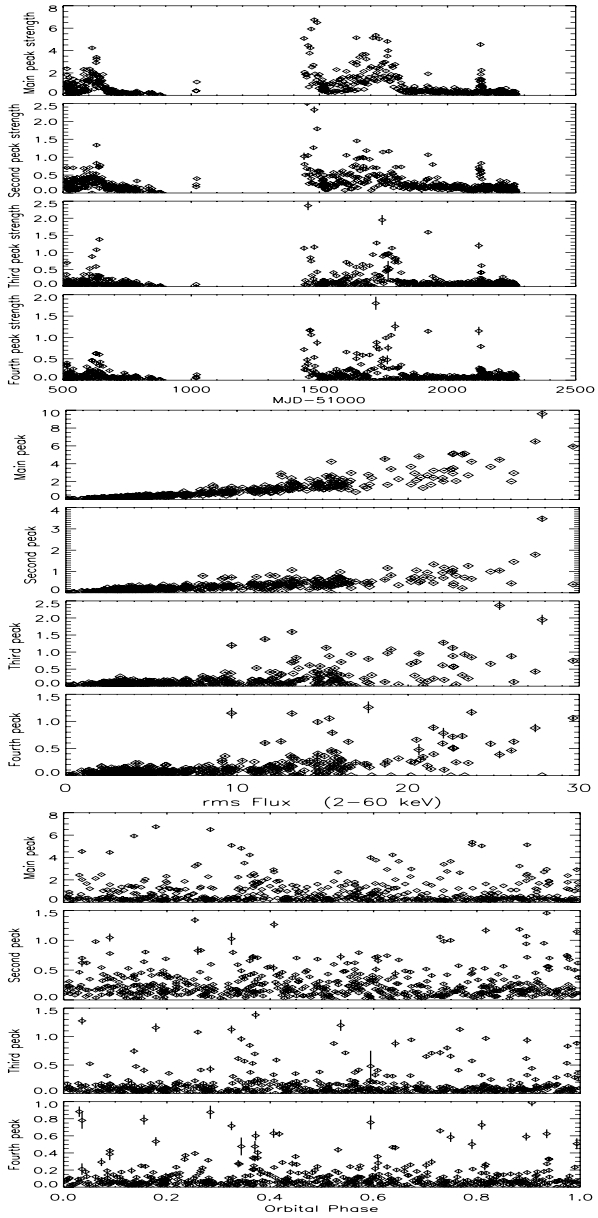

Fig. 5. We have obtained 2–60 keV *RXTE* PCA pulse shapes varying from only single sinusoidal-like peak (phases 0.9–1), to profiles with two peaks (phases 0.7–0.9), and even occasionally with three (phases 0.5–0.7) and four peaks (0.2–0.5). From top to bottom, the four peaks strength is plotted vs. time, luminosity (2–60 keV rms flux) and orbital phase.

from one to three peaks in addition to the main one. The general behavior is:

1. the right side of the main peak (phases 0.0–0.2) remains quite similar as energy increases;
2. the region at phases 0.2–0.5 is not always a peak. But when a peak is present then it tends to strengthen as energy increases;
3. when a peak is present at phases 0.5–0.7, the larger is the energy the weaker is the feature;
4. at phases 0.7 to 0.9 a secondary peak or shoulder is present. It gets smaller with increasing energy;
5. the dip in the main peak (phase 0.9) becomes deeper as the energy range increases. The maximum depth is found in the 7.76–13.93 keV band, and then decreases again with energy.

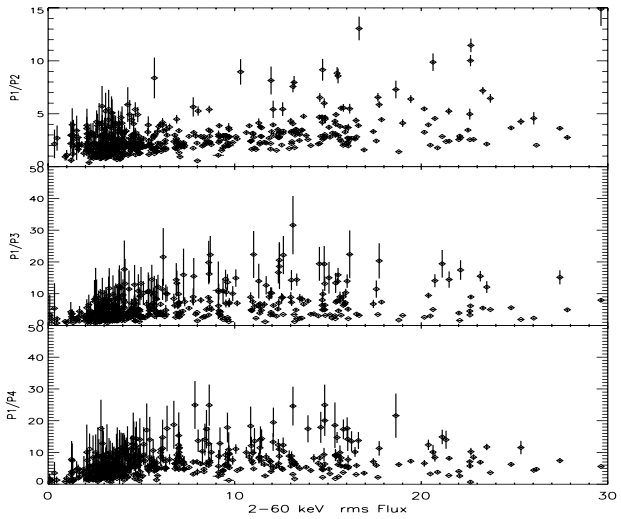

Fig. 6. *From top to bottom*, the ratio of the main to the second, the third and the fourth peak plotted vs. luminosity (2–60 keV rms flux). We have rejected few observations with large uncertainties for clarity.

In particular, observations 70082-03-16-00 and 70082-04-57-00 show this notch especially deep and wide, the last one evolving to a strong double peak (see Figs. 7 and 8).

This trend is also seen in the 20–60 keV IBIS/ISGRI profiles (see Fig. 9), where the second and the third peaks are almost missing and the fourth one is stronger, but still weaker than the main peak. It should be noted that in Fig. 9, the profile in the upper left is substantially offset from phase 1.0. The reason is that all of these profiles are arbitrary pulse phased and are not phase aligned with one another, hence there is no reason for them to be close in phase. The two profiles on the right are rather close in time to each other, so the phases of the main peak are similar while the ones on the left are more widely spaced in time.

The averaged strength of the main and the rest of the peaks have been plotted vs. energy band in Fig. 10. We can see the peaks evolution with energy suggested in points 1 to 5.

3.2. Spectral analysis

We have obtained 548 spectra from 6 years of *RXTE* PCA and HEXTE data (MJD 51 512.8 – MJD 53 047.9). For each observation, we have selected PCA Standard2 data and HEXTE binned mode data from clusters A and B. Then, fluxes in all the different energy ranges were obtained by fitting a cut-off power law model plus a photoelectric absorption (phabs×(Gauss + cutoffpl)) to each 2.7–70 keV spectrum, fixing the iron line value and its width to 6.43 keV and 0.165, respectively (Baykal et al. 2002). We have included 1% of systematics. They were also background subtracted.

In Fig. 12 (bottom) we show the long-term flux history of SAX J2103.5+4545 using *RXTE* and *INTEGRAL* data, which follows very nicely the general trend of the long-term frequency derivatives history obtained after the timing analysis (see next section).

To study the spectral variability of SAX J2103.5+4545 we have computed the long-term hardness ratios (HR) using two energy bands: 2–10 keV, 10–30 keV (defined as $HR = H/S$). Figure 11 (top) shows an average of the calculated HR vs. time and intensity, using those energy bands. In the HR vs. intensity plot we took out few detections corresponding to

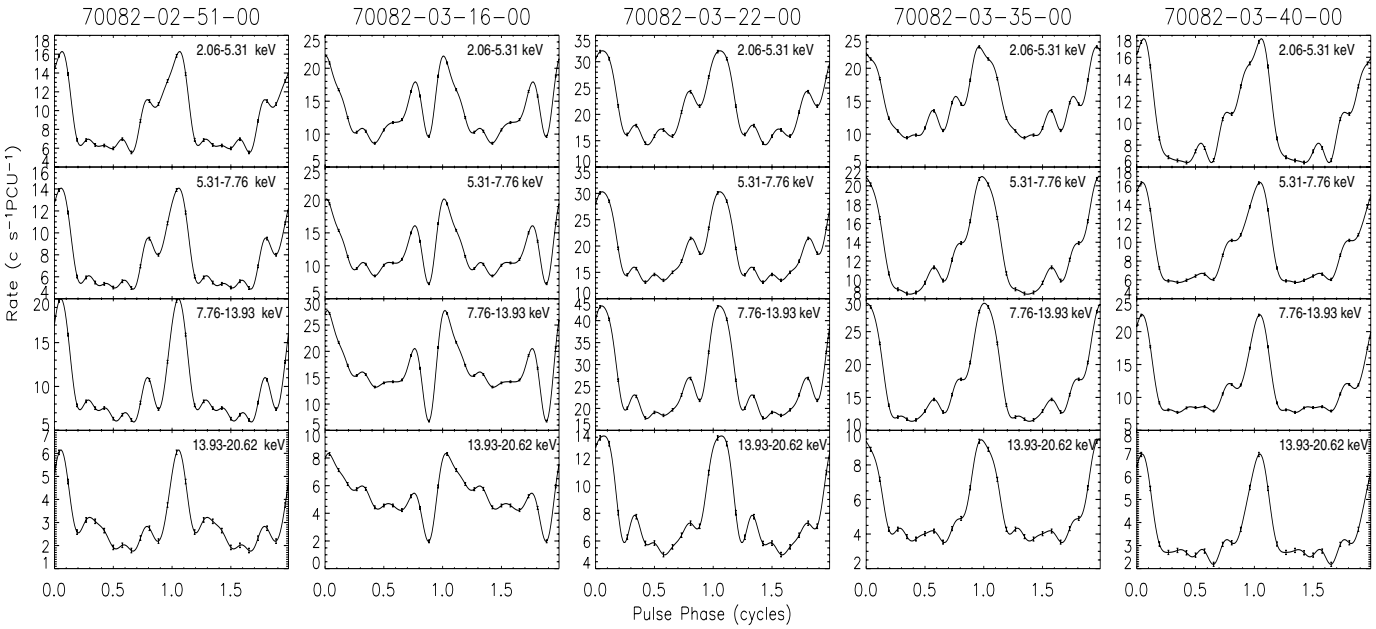

Fig. 7. Evolution of SAX J2103.5+4545 PCA pulse profile with intensity in 4 energy bands (*from top to bottom*). They are sorted consecutive in time during the brightest period (MJD 52 650–52 800) of the source.

the faintest state, due to their enormous error bars, which hid the general trend. The correlation between the HR either with time or intensity is clear. We can see that the source becomes harder when the flux is higher. In the same figure we have included some plots showing the evolution of the absorption, the Photon Index, the cutoff and the reduced χ^2 with intensity. We have also rejected the faintest flux values since the uncertainties obtained in the parameters were very large, adding only confusion to the study. We found variable behavior only in the Photon Index vs. intensity plot. The larger the flux the lower the the photon index. This anti-correlation was the expected and shows again that in the bright state the spectrum of SAX J2103.5+4545 is harder than in the faint state. It is clear that the fitting model applied is not the perfect one for the bright state, as we can see in the reduced χ^2 vs. intensity figure. Nevertheless, it was found to be the best simple model for all the ∼500 spectra analyzed. Baykal et al. (2007) suggested that this type of spectral softening with decreasing flux was found to be mainly a consequence of mass accretion rate change and was not necessary to be related to a significant accretion geometry change.

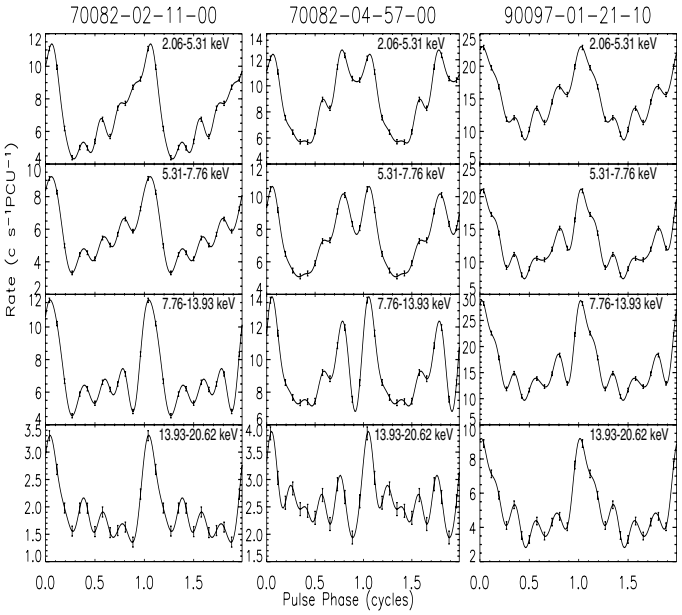

Fig. 8. Some examples of SAX J2103.5+4545 PCA pulse profiles showing a more complex structure, in the same 4 energy bands.

3.3. Timing analysis

3.3.1. Phasing

We selected again the 548 *RXTE* PCA observations for the long-term timing analysis. Then we obtained either a list of good events times per science window (*INTEGRAL* IBIS/ISGRI, 20–60 keV) or binned light curves (*RXTE* PCA, 2–60 keV). The times were corrected to the barycenter of the solar system and for the orbital motion. We constructed pulse profiles in those energy bands by fitting the data with a harmonic expansion in pulse phase, as we described in the pulse profile section. Initially we used the same simple phase model and the errors on the Fourier coefficients were corrected for the non-Poisson noise.

The profiles were grouped into 12.69 d intervals with frequencies and frequencies derivatives being estimated for each interval using a grid search of the Y_n statistics (Finger et al. 1999). The measured frequencies were then fitted with a piecewise-linear model. Then the profiles were remade using the integral of the fitted frequency model as a phase model.

For the *INTEGRAL* IBIS/ISGRI data the approach was different, due to the non continuous observational pattern and the sensitivity of the ISGRI detector (see Table 1). A template profile was then created from the average profile from the set of ISGRI ScWs and from the collected pulse profiles from the *RXTE* PCA data. To generate phase offsets from the model, we then cross-correlated the individual profiles with the template profiles. The new phases (model + offset) were then fitted with a quadratic-spine phase model, which was used to remake the profiles. New phase offsets were then estimated.

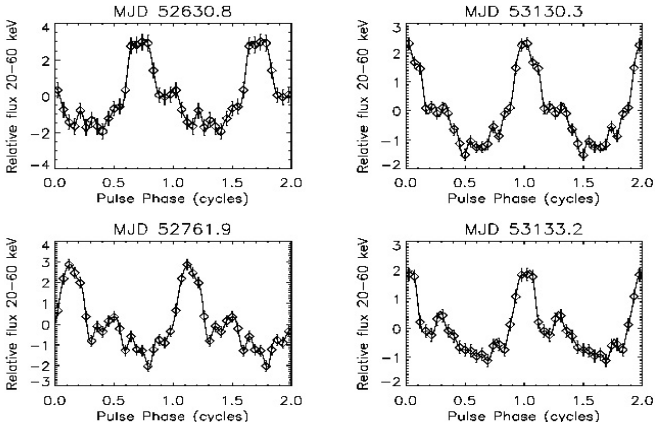

Fig. 9. ISGRI (20–60 keV) mean pulse profiles of SAX J2103.5+4545 generated by combining profiles from individual *INTEGRAL* ScWs.

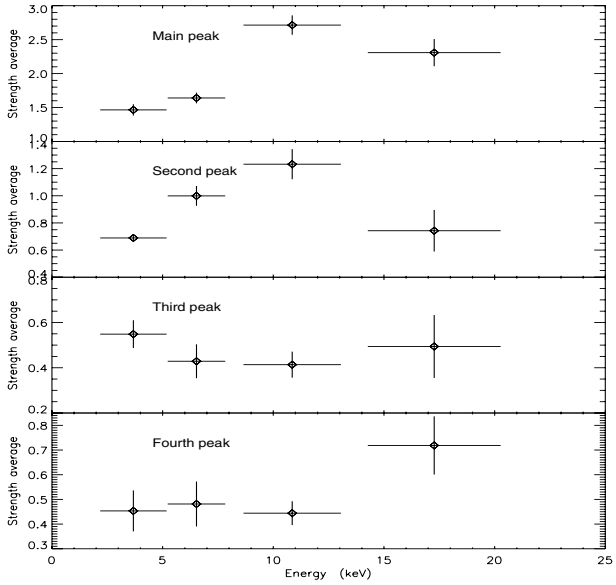

Fig. 10. Averaged peaks strength evolution with energy. The behaviour displayed here follows the one proposed from points 1 to 5 in the text.

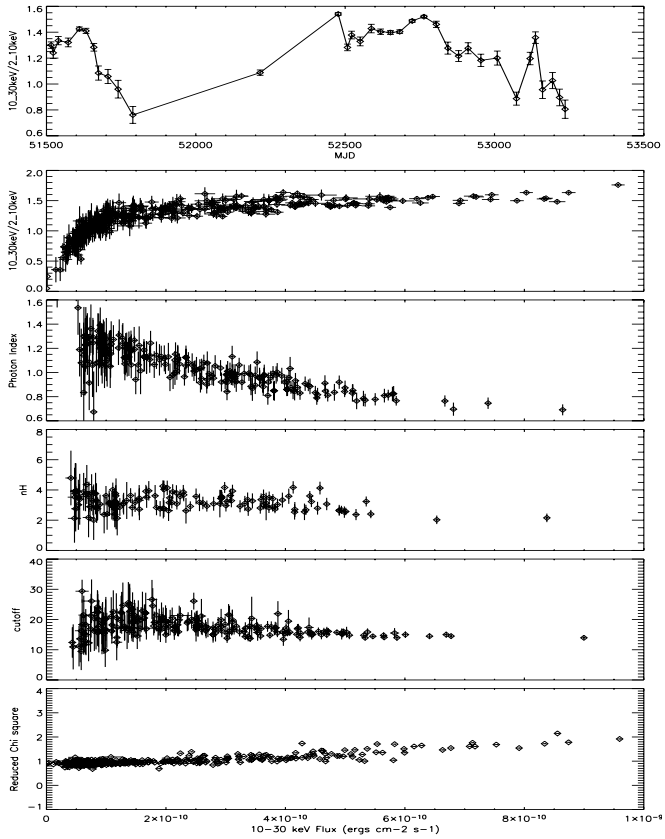

Fig. 11. *Top.* Long-term hardness ratios history. From *middle to bottom*: HR-intensity diagram and spectral parameters evolution vs. intensity.

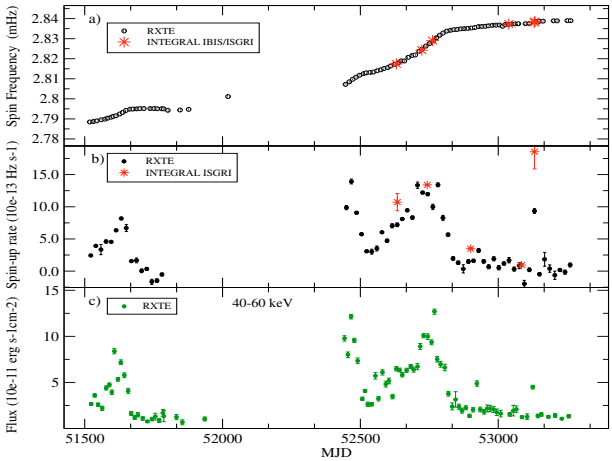

Fig. 12. *Top*: long-term frequency history. *Middle*: averaged spin-up rates history. *Bottom*: 40–60 keV *RXTE* HEXTE averaged fluxes. A spin-up rate and X-ray flux correlation was found, confirming that an accretion disk during periastron passage is present.

Figure 12 shows the long-term spin-frequency and spin-up rate history obtained after repeating the grid search with the new profiles and phases. For IBIS/ISGRI the spin rates were computed by differencing adjacent frequency measurements and dividing by the corresponding time difference. The PCA spin rates were computed by fitting a quadratic function to the phases, which were divided in 29 time intervals. We see that the first outburst of SAX J2103.5+4545 started with a spin-up trend (bright state), made a transition to a steady spin rate (faint state), and then appeared to begin a spin-down trend. The following available data started with a quick spin-up trend (bright state), and then a transition to a slower spin-up rate (faint state).

Comparing the fluxes obtained in the non averaged long–term light curve (the one composed of around 500 individual flux measurements from the spectra; see bottom of Fig. 4), we realized that while SAX J2103.5+4545 was in the faint state (MJD 53 100), suddenly it increased dramatically its luminosity for a short time period. This was not the first episode of such a behavior but the strongest one. Therefore, the ISGRI frequency derivative outlier cannot be ruled out since it seems it is related to a significant event.

3.3.2. Orbit fitting

Errors in the orbital parameters caused by coupling between the intrinsic spin variations of the pulsar with orbital effects, can scatter the detected pulse frequencies. In order to achieve a better characterization of the geometry of this binary system, we

Table 2. Orbital solution for SAX J2103.5+4545.

	Baykal et al. (2002)	İnam et al. (2004)	Sidoli et al. (2005)	Baykal et al. (2007)	Present work
$T_{\pi/2}$ (MJD)	51 519.3 ± 0.2	52 633.90 ± 0.05		52 469.336 ± 0.057	52 545.411 ± 0.024
$P_{\rm orb}$ (days)	12.68 ± 0.25		12.670 ± 0.005	12.66536 ± 0.00088	12.66528 ± 0.00051
$a_x \sin i$ (lt-s)	72 ± 6			74.07 ± 0.86	80.81 ± 0.67
e	0.4 ± 0.2			0.4055 ± 0.0032	0.401 ± 0.018
ω (deg)	240 ± 30			244.3 ± 6.0	241.36 ± 2.18

have used *RXTE* PCA Standard1 data to obtain a new set of orbital parameters. To take into account the phase noise caused by pulse profile variations we split the *RXTE* results into 29 intervals (3 orbits) and fitted an orbit to the phases in each interval (the orbital Period was fixed). The fitting model for each interval consisted of a quadratic phase model combined with an orbital model parametrized by the elements $a_x \sin i$, $g = e \sin(\omega)$, $h = e \cos(\omega)$, and $T_{\pi/2}$, with the orbital period $P_{\rm orb}$ fixed, and the epoch $T_{\pi/2}$ placed near the middle of the interval. Where $T_{\pi/2}$ is the epoch when the mean orbital longitude is equal to 90 deg, $P_{\rm orb}$ is the orbital period, $a_x \sin i/c$ is the light-travel time for the projected semi-major axis (i is the inclination angle), e is the eccentricity and ω is the longitude of periastron.

The final orbital parameters were obtained from a unweighted average of the best fit parameters from just 28 intervals. As we mentioned above, taking a look at the long-term light curve we noticed that around MJD 53 100 a huge and narrow spike occurred while the source was in the faint state. This surprising behavior was also noticed in orbital fit number 26, resulting in a highly dispersed fit that was finally rejected. The final orbital epoch and period were obtained by making a linear fit to the 28 best fit orbital epochs. The errors in these parameters were estimated from the scatter of the best fit parameters. Finally the eccentricity e and argument of periastron ω where obtained from the average values of g and h. Table 2 lists the final orbital parameters obtained.

Our orbital parameters agree within errors with those obtained by Baykal et al. (2007) with the exception of $a_x \sin i$, where our value is $\sim 7\sigma$ larger than theirs. Since both results were obtained from essentially the same data set, the difference must be due to the different approaches taken in the analysis. Baykal et al. analyzed data from 11 intervals of varying size which where fit with a global orbital model, with independent 5th order phase models for each interval. We made local orbital fits for 28 intervals of three orbit duration including a second order phase model with each, and then averaged the local orbital parameters to obtain a mean orbit model. This method of averaging local orbits was introduced by Boynton et al. (1986) so that the errors in the orbital elements introduced by random torque variations could be empirically accounted for. Here however the torque variations are not random, but are correlated with the flux, which at higher flux levels is correlated with orbital phase. One possibility is that some of the orbital signature is being absorbed into the phase model used for each interval in the Baykal et al. analysis, which contains 4 parameters to describe the intrinsic torque during the each interval. The Baykal et al. analysis used on average 0.55 torque parameters per binary orbit, while our torque models were stiffer, using 0.33 torque parameters per orbits. In addition, the shortest intervals in the Baykal analysis, which used up to 1.9 torque parameters per orbit, tended to occur at the highest flux levels, where the data has more weight in the global fit. Out of 28 estimations of $a_x \sin i$ we find only two that have values below the Baykal et al. value.

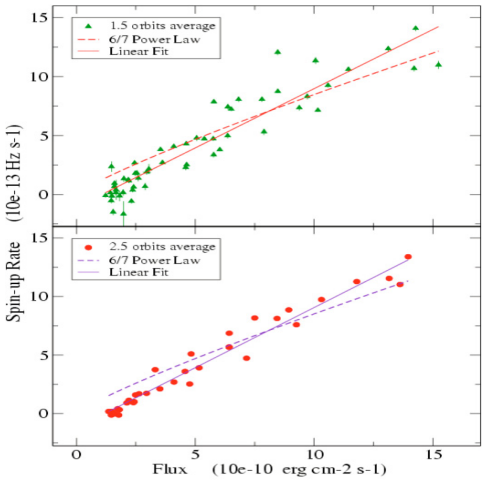

Fig. 13. Spin-up rates vs. *RXTE* 2–100 keV non absorbed averaged flux every 1.5 and 2.5 orbits. A linear fit was found the best one.

3.3.3. Spin-up torque-flux correlations

We averaged the non absorbed flux every 1.5 and 2.5 pulsar orbits. The 1.5 orbits average is the smallest time interval that allowed us to fit a quadratic function to the phases when the spin rates were computed. The second time interval of 2.5 orbits was chosen as a good representative of the general trend. Figure 13 shows more clearly the spin-up rate vs. flux correlation. We have fitted both data sets with a single power law (*solid line*). In the same figure, a dashed line denotes our best-fit power law with an index fixed at 6/7, which represents the relationship between spin-up and flux predicted by simple accretion theory.

In principle, Fig. 13 seems to be nearly identical to Fig. 5 from Baykal et al. (2007), and our results confirm those found by them. However, we believe that an interesting feature should be emphasized. Data averaging over 1.5 orbits scatters more than averaging over 2.5 orbits. It appears that the smaller is the average the bigger is the scattering. This might suggest that, in addition to the disk accretion mechanism, there seems to exist another mechanism producing erratic variations.

4. Discussion

4.1. The Pulse profile

Some X-ray pulsars, like EXO 2030+375 (Parmar et al. 1989), show a clear pulse shape dependence on source luminosity, most likely controlled by accretion rate. Differences in X-ray pulse profiles are considered to be due to the differences in the geometrical configuration with respect to the rotational axis of the neutron star, the axis of magnetic dipole moment, and the observer's line of sight (Nagase 1989). The structure of the accretion column determines the basic

profile of the pulse pattern. However, simple geometric models with two pencil beams coming from the magnetic poles or two bright spots on the neutron star surface, cannot explain the variability observed in some other systems, like Vela X–1. Previous studies by Kreykenbohm et al. (2002) confirmed for Vela X-1 a very complex pulse profile at low energies (below 6 keV), showing a five peak structure. Above 10 keV the pulse profiles evolved into a simple double peak. They pointed out that a good description of the processes responsible for the complex shape at low energies is still missing.

In the present work, the 2–60 keV SAX J2103.5+4545 pulse shapes obtained with *RXTE* PCA were found to be peculiarly complex and variable either with luminosity, time or orbital phase. For the first time the pulse shapes seem to vary randomly from not only single sinusoidal-like peak but profiles with two, three and even occasionally four peaks, with no evident interrelationship. For a given energy range, temporal variability of the pulse profile of SAX J2103.5+4545 was explained by Sidoli et al. (2005) as likely due to a time-dependent emission pattern, or to changes in the opacity of the magnetized plasma through which the radiation propagates.

Previous works by Baykal et al. (2002), Falanga et al. (2005) and Sidoli et al. (2005) obtained a single peak pulse profile in soft X-ray bands, using *RXTE* and *INTEGRAL* data. However, İnam et al. (2004) found a double peak profile using *XMM-Newton*, but this exception could be compatible with the variability seen in our study for SAX J2103.5+4545.

In the hard X-ray range, we have obtained much simpler double peak profiles 20–40 keV *INTEGRAL* ISGRI profiles, in agreement with previous results by Falanga et al. (2005) and Sidoli et al. (2005). Filippova et al. (2004) published a 20–100 keV single peak pulse profile using PV phase *INTEGRAL* data. Taking into account the uncertainties in their results, this could be compatible with our PV phase results (see Fig. 9, MJD 52 630 pulse profile).

In addition, our study allowed us to confirm an energy dependence pattern for SAX J2103.5+4545. Unfortunately, as in Vela X–1, we did not find out a straightforward explanation for the low energy pulse profiles. İnam et al. (2004) found practically no variation in the energy dependence of the 0.9–11 keV pulse profiles, which is not in agreement with our results. Falanga et al. (2005) obtained an energy dependent secondary peak around phase 0.2, which became more evident at energies above 20 keV. This peak might be compatible with the evolution of our peak at phase 0.7. They also claimed that at phase 0.6 some very short variation features (hicc-ups) were present, in agreement with those observed by İnam et al. (2004) using *XMM-Newton* data. These "hicc-ups" were only visible at high energies (40–80 keV). Again, these features might be compatible with our dip at phase 0.9.

It is generally accepted that in order to explain the energy-dependent changes seen in the pulse profile, the anisotropic radiation transfer must be taken into account (Nagase 1989). Previous studies by Krauss et al. (2003) found that energy-dependent peaks in medium luminosity binary X-ray pulsars, are mainly due to the energy-dependent relative importance of the halo (which forms around the accretion funnel where the neutron star surface is irradiated) and the column contributions to the observed flux (Sidoli et al. 2005). For SAX J2103.5+4545, Falanga et al. (2005) found that changes in the morphology of the pulse profile as a function of energy were consistent with variations in the spectral components visible in their pulse phase resolved spectra analysis. Their study also showed that differences in the double-peak can be modeled by a different scattering fraction between the radiation from the two magnetic poles.

4.2. Nature of the source

First studies of SAX J2103.5+4545 by Baykal et al. (2002) showed a transition from spin-up to spin-down in the *RXTE* observations from an outburst in November 1999, suggesting the presence of an accretion disk. The detection of a quasi-periodic oscillation at 22.7 s discovered by İnam et al. in 2004, provided further evidence for its existence. The spin-up rate and X-ray flux correlation is also observed in the present work, confirming that an accretion disk is present during periastron passage. Previous works by İnam et al. (2004) and Baykal et al. (2002, 2007) are in good agreement with our results. In general, either the pulse period estimations from Sidoli et al. (2005) or those ones from Blay et al. (2006) are not in very good agreement with our results.

An accretion disk will form if the specific angular momentum of the accreted material ℓ is comparable to the Keplerian specific angular momentum at the magnetospheric radius $\ell_{\rm m}$. To estimate ℓ for SAX J2103.5+4545, we assumed typical pulsar parameters, and typical values of $\dot{\nu} \simeq 7 \times 10^{-13}$ Hz s^{-1}, $F \simeq 7 \times 10^{-10}$ erg cm^{-2} s^{-1} (see Fig. 13) (Wilson et al. 2003, 2005 and references therein). The distance of the source from optical observations is 6.5 ± 0.9 kpc (Reig et al. 2004, 2005). Several authors have discussed a possible value for the magnetic field. Recently, Baykal et al. (2007) obtained a value of 16.5×10^{12} Gauss. But this implied a distance of 4.5 kpc. In order to explain the spin-up rate observed, and assuming that the distance of 6.5 kpc is correct, Sidoli et al. (2005) obtained a magnetic field of $\sim 1.6 \times 10^{12}$ Gauss. No cyclotron lines have been observed from this source. One explanation could be a high magnetic field as proposed by Baykal et al. (2007) which would imply a fundamental line at ∼200 keV.

We have summarized in Table 3 the different values obtained for ℓ, using the two magnetic field measurements discussed above, assuming two distance values of 6.5 kpc and 4.5 kpc, and for $k = 0.91$ (simple spherical accretion model) and 0.47 (Ghosh & Lamb 1979, model). As expected, all cases confirm that a disk is likely to be present. Only those cases with lower ℓ/ℓ_m ratio might indicate that alternating periods of wind accretion and disk accretion could also take place in this system.

It is generally accepted that the propeller effect is likely connected to quiescence states. Reig et al. (2005, and references therein) stated as possible values for the threshold X-ray luminosity $\sim 10^{32}$–10^{33} erg s^{-1}. Unusually, from photometric and spectroscopic observations performed in 2004 (Reig et al. 2005) and during the faint state of this source, SAX J2103.5+4545 continued emitting X-rays even after having completely lost the disk.

To determine whether or not centrifugal inhibition of accretion is operating, we estimated the flux at the onset of this effect by equating the magnetospheric radius to the corotation radius. For SAX J2103.5+4545 the threshold flux for the onset of centrifugal inhibition of accretion, i.e.,

$$F_{\rm min} \simeq 2 \times 10^{-12} \text{ erg cm}^{-2} \text{ s}^{-1} \times k^{7/2} \mu_{30}^2 M_{1.4}^{-2/3} R_6^{-1} P_{354.9s}^{-7/3} d_{\rm kpc}^{-2} \quad (1)$$

where μ_{30}, $M_{1.4}$, R_6, and $P_{354.9}$ are the pulsar's magnetic moment in units of 10^{30} G cm^3, mass in units of 1.4 $M_\odot$, radius in units of 10^6 cm, and spin period in units of 354.9 s, respectively. Table 3 shows our measured $F_{\rm min}$ using Eq. (1). Our observed upper limit fluxes are in the range $\simeq$(5–0.9)$\times 10^{-12}$ erg cm^{-2} s^{-1},

Table 3. Comparison of the specific angular momentum of the accreted material to the Keplerian specific angular momentum at the magnetospheric radius. An estimation of the flux for the onset of centrifugal inhibition of accretion is also shown.

	$B = 16.5 \times 10^{12}$ G (4.5–6.5) kpc	$B = 1.65 \times 10^{12}$ G (4.5–6.5) kpc
$k = 0.91$	$\ell = (0.61–0.33)\ \ell_m$	$\ell = (1.19–0.63)\ \ell_m$
	$F^*_{\rm min} = (20.4–9.8)$	$F^*_{\rm min} = (0.2–0.097)$
$k = 0.47$	$\ell = (0.85–0.45)\ \ell_m$	$\ell = (1.65–0.88)\ \ell_m$
	$F^*_{\rm min} = (2.02–0.97)$	$F^*_{\rm min} = (0.02–0.0097)$

$^* \times 10^{-12}$ erg cm^{-2} s^{-1}.

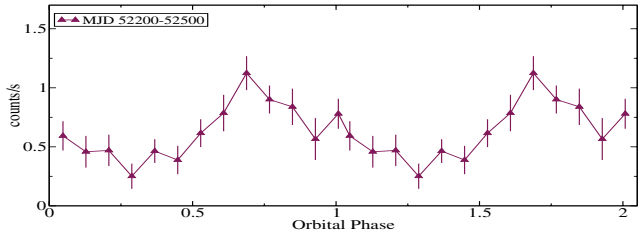

Fig. 14. *RXTE* ASM orbital light curve of SAX J2103.5+4545 from MJD 52 200–52 500.

consistent with SAX J2103.5+4545 entering the centrifugal inhibition of accretion regime only for $B = 16.5 \times 10^{12}$ G (see Table 3).

In principle, as Reig et al. (2005, and references therein) pointed out, it is still possible to produce X-rays when the propeller effect is working (e.g. through accretion onto the magnetosphere as opposed to onto the neutron star surface or through leakage through the magnetosphere). However, due to the fact that SAX J2103.5+4545 is located in the region of wind-fed supergiant binaries in the $P_{\rm spin}$–$P_{\rm orb}$ diagram, accretion from the stellar wind of the B0 companion might be the origin of the observed luminosity. Reig et al. (2005) closed their work saying that the relatively narrow orbit of SAX J2103.5+4545 implies that the wind, at the position of the neutron star, does not reach its terminal velocity, but varies in the range ∼[0.7–0.9].

4.3. Transient vs. persistent

Up to now, SAX J2103.5+4545 has been classified as a transient Be/X-ray binary system. However, as we stated above, this source is a very interesting case. Maybe, its location in the wind-fed supergiant region might also be the origin of its complex pulse profile behavior. It should be noted that a large population of persistent, likely wind-accreting supergiants are being discovered by the *INTEGRAL* mission.

In the present work SAX J2103.5+4545 was detected clearly in all our observations, hence there is no well-defined limit dividing outbursting vs. quiescence. Defining a threshold for the observed flux at 5×10^{-12} erg cm^{-2} s^{-1}, we can identify 5 outbursts from Fig. 4 (bottom). Ignoring the fact that the luminosity never exceeds 10^{37} erg cm^{-2} s^{-1}, the first three might qualify as type II outbursts because: a) they last for multiple orbits, b) there is only moderate orbital modulation (see Fig. 14), c) there is a flux-spin up correlation. The last two outbursts are short and could be considered as type I. In the "quiescence" state where the luminosity is $\sim 10^{35}$ erg cm^{-2} s^{-1}, we see a gradual flux decline after the third "type II" outburst, yet the frequency continues to increase. This is again not typical, but it has been seen in other wind-fed systems (Bildsten et al. 1997). Overall, the behavior of the source does not fit well with the standard picture of Be/X-ray transients. We also believe that this peculiar Be/X-ray system with the narrowest of orbits, may be classified as a Persistent (but highly variable) source.

Acknowledgements. We thank Peter Kretschmar for very useful comments and his support. We appreciate the very useful comments from the referee, which have helped us to improve the paper. We also would like to thank to NASA Marshall Space Flight Center, the National Space Science Technology Center and the Universities Space Research Association for the opportunity to develop the present work. This research is supported by the Spanish Ministerio de Educación y Ciencia through grant-no ESP2002-04124-C03-02. Thank also to Paul Connell for his support.

References

Baykal, A., Stark, M. J., & Swank, J. H. 2000, ApJ, 544, L129
Baykal, A., Stark, M. J., & Swank, J. H. 2002, ApJ, 569, 903
Baykal, A., İnam, S. ÃĞ., Stark, M. J., et al. 2007, MNRAS, 374, 1108
Blay, P. 2006, Ph.D. Thesis work, Multiwavelength Analysis of two peculiar High Mass X-ray binary systems: 4U 2206+45 and SAX J2103.5+4545. New insights from INTEGRAL
Blay, P., Reig, P., Martínez Núñez, S., & Camero, A. 2004, A&A, 427,293
Boynton, P. E., Deeter, J. E., Lamb, F. K., & Zylstra, G. 1986, ApJ, 307, 545
Bradt, H. V., Rothschild, R. E., & Swank, J. H. 1993, A&AS, 97, 355
Camero Arranz, A., Wilson, C. A., Finger, M. H., & Reglero, V. 2006, Proc. 6th *INTEGRAL* Workshop, in press
Courvoisier, T. J.-L., Walter, R., Beckmann, V., et al. 2003, A&A, 411, L53
Diehl, R., Baby, N., Beckmann, V., et al. 2003, A&A, 411, L117
Falanga, M., di Salvo, T., Burderi, L., & Bonnet-Bidaud, J. M. 2005, A&A, 436, 313
Filippova, E. V., Lutovinov, A. A., Shtykovsky, P. E., et al. 2004, Astron. Lett., 30, 12, 824
Finger, M. H., Wilson, R. B., Chakrabarty, D., et al. 1996, A&AS, 120, 209
Finger, M. H., Bildsten, L., Chakrabarty, D., et al. 1999, ApJ, 517, 449
Ghosh, P., & Lamb, F. K. 1979, ApJ, 234, 296
Goldwurm, A., David, P., Foschini, L., et al. 2003, A&A, 411, L223
Gruber, D. E., Blanco, P. R., Heindl, W. A., et al. 1996, A&AS, 120, 641
Hulleman, F., in 't Zand, J. J. M., & Heise, J. 1998, A&A, 337, L25
Illarionov, A. F., & Sunyaev, R. A. 1975, A&A, 39, 185
İnam, S. Ã., Baykal, A., Swank, J., & Stark, M. J. 2004, ApJ, 616, 463
Jahoda, K., Swank, J., Giles, A. B., et al. 1996, Proc. SPIE, 2808, 59
Kraus, U., Zahn, C., Weth, C., & Ruder, H. 2003, ApJ, 590, 424
Kreykenbohm, I., Coburn, W., Wilms, J., et al. 2002, A&A, 395, 129
Lamb, F. K., Pethick, C. J., & Pines, D. 1973, ApJ, 184, 271
Levine, A. M., Bradt, H., Cui, W., et al. 1996, ApJ, 469, L33
Nagase, F. 1989, Publ. Astron. Soc. Japan, 41, 1
Parmar, A. N., White, N. E., Stella, L., et al. 1989, ApJ, 338, 373
Pringle, J. E., & Rees, M. J. 1972, A&A, 312, 872
Reig, P., Negueruela, I., Fabregat, J., et al. 2004, A&A, 421, 673
Reig, P., Negueruela, I., Papamastorakis, G., et al. 2005, A&A, 440, 637
Sidoli, L., Mereghetti, S., Larsson, S., & Chernyakova, M. 2004, Proc. 5th *INTEGRAL* Workshop, ESA SP-552, 475
Sidoli, L., Mereghetti, S., Larsson, S., & Chernyakova, M. 2005, A&A, 440, 1033S
Stollberg, M. T., Finger, M. H., Wilson, R. B., et al. 1999, ApJ, 512, 313
Westergaard, N. J., Kretschmar, P., Oxborrow, C. A., et al. 2003, A&A, 411, L257
Wilson, C. A., Finger, M. H., Harmon, B. A., et al. 1997, ApJ, 479, 388
Wilson, C. A., Finger, M. H., Coe, M. J., Laycock, S., & Fabregat, J. 2002, ApJ, 570, 287
Wilson, C. A., Finger, M. H., Coe, M. J., & Negueruela, I. 2003, ApJ, 584, 996
Wilson, C. A., Fabregat, J., & Coburn, W. 2005, ApJ, 620, L99